SOFT ROBOTS

# A soft, bistable valve for autonomous control of soft actuators



Philipp Rothemund,[1,2,3] Alar Ainla,[2] Lee Belding,[2] Daniel J. Preston,[2] Sarah Kurihara,[2] Zhigang Suo,[1,3] George M. Whitesides[2,3,4]*

**Almost all pneumatic and hydraulic actuators useful for mesoscale functions rely on hard valves for control. This article describes a soft, elastomeric valve that contains a bistable membrane, which acts as a mechanical "switch" to control air flow. A structural instability—often called "snap-through"—enables rapid transition between two stable states of the membrane. The snap-upward pressure, $\Delta P_1$ (kilopascals), of the membrane differs from the snap-downward pressure, $\Delta P_2$ (kilopascals). The values $\Delta P_1$ and $\Delta P_2$ can be designed by changing the geometry and the material of the membrane. The valve does not require power to remain in either "open" or "closed" states (although switching does require energy), can be designed to be bistable, and can remain in either state without further applied pressure. When integrated in a feedback pneumatic circuit, the valve functions as a pneumatic oscillator (between the pressures $\Delta P_1$ and $\Delta P_2$), generating periodic motion using air from a single source of constant pressure. The valve, as a component of pneumatic circuits, enables (i) a gripper to grasp a ball autonomously and (ii) autonomous earthworm-like locomotion using an air source of constant pressure. These valves are fabricated using straightforward molding and offer a way of integrating simple control and logic functions directly into soft actuators and robots.**

## INTRODUCTION

Pneumatically actuated soft robots function by networks of elastomeric channels that inflate upon pressurization or buckle upon evacuation (*1*–*6*). Soft devices, and their actuators, are intrinsically compliant and can move in ways that are difficult or impossible to achieve using "hard" components. Other useful characteristics of soft actuators and devices include (i) collaborative behavior, that is, intrinsic safety in operating closely with humans (*6*–*8*); (ii) the ability to adapt autonomously to different shapes (*1*, *9*); (iii) relatively low cost (*6*, *8*); (iv) ease of sterilization (*10*); (v) the ability to manipulate delicate objects (*1*, *11*); and (vi) high cycle lifetime (*4*). One characteristic (and deficiency, in some applications) of most current soft, pneumatic actuators is that they still rely on hard valves and electronic components for control (*8*).

Elastomers undergo large deformations, which enable functions but also present challenges in design. Precisely controlling the motion of soft, pneumatic actuators can be difficult, because elastomers are often nonlinear and viscoelastic (*6*, *9*, *12*). Control is further complicated by the need for sensors that can sustain the same strain as the actuators (*11*, *13*–*15*). The compliance of the elastomers allows the devices to conform to different shapes and automatically limits the force they exert (a form of "material intelligence") (*8*, *16*). These characteristics enable them to operate in many applications between pressure limit set points. These set points allow soft actuators to be controlled with the simple on/off of a pressure supply. Grippers and walkers are two examples of successful applications operating with this type of pressure control (*1*, *2*, *17*).

The most common methods of controlling pressure in soft robots involve hard valves (e.g., solenoid valves) that open or close in response to a pneumatic or electronic signal (*8*, *9*, *18*). Wood and coworkers (*19*) developed a band-pass valve, which can address multiple actuators individually using a single, modulated source of pressure. Marchese *et al.* (*20*) developed an energy-efficient valve based on electropermanent magnets. We used a Braille display in combination with a microfluidic circuit to control 32 actuators simultaneously (*21*). Each of these valves contains hard components and is usually located externally; this architecture requires tethering the robot with tubing. Hard valves have been integrated onto soft robots, sacrificing complete softness (*18*, *20*). Some attempts have been made to fabricate a soft controller (i.e., a "switch" or other logic element) specifically for soft robots. We have directly integrated unidirectional, soft check valves into a soft robot to vent the combustion products of an explosion, which powered the soft robot (*22*). Wehner *et al.* (*23*) developed an entirely soft, autonomous robot, which was controlled by a soft microfluidic oscillator based on a design first introduced by Takayama and coworkers (*24*).

Many designs exist for entirely soft microfluidic valves, logic circuits, oscillators, and fluidic information processors (*24*–*27*). These designs use Quake-type valves, in which elastomeric membranes block or permit flow through channels depending on an applied input pressure (*27*). A microfluidic oscillator relies on a network of fluidic components, which include valves (switches), channels (resistors), chambers (capacitors), and pressure sources (*24*, *28*). The dimensions of the components must be balanced to achieve oscillatory behavior of the circuit. Hui and coworkers (*28*) demonstrated complex microfluidic circuits with a high density of logic elements. The small scale of the microfluidic circuit used by Wehner *et al.* (*23*) limited the flow rate, and thus the size, of the actuator that could be controlled. They overcame this problem to some extent by operating the microfluidic circuit with liquid $H_2O_2$, which generated, catalyzed by platinum, gaseous $O_2$ inside the robot to increase the volume (*23*). The small feature sizes of the microfluidic channels also required the use of multiple fabrication techniques [soft lithography (*27*, *29*), three-dimensional (3D) printing, and molding] and led to difficulties (clogging of the channels) when interfacing the microfluidic channels with the channels of the robot (*23*).

This paper describes a type of soft valve that uses the snap-through instability of an elastomeric membrane to switch between different pneumatic pressures to control the airflow through pneumatic channels.

[1]John A. Paulson School of Engineering and Applied Sciences, Harvard University, 29 Oxford Street, Cambridge, MA 02138, USA. [2]Department of Chemistry and Chemical Biology, Harvard University, 12 Oxford Street, Cambridge, MA 02138, USA. [3]Kavli Institute for Bionano Science and Technology, Harvard University, 29 Oxford Street, Cambridge, MA 02138, USA. [4]Wyss Institute of Biologically Inspired Engineering, 60 Oxford Street, Cambridge, MA 02138, USA.
*Corresponding author. Email: gwhitesides@gmwgroup.harvard.edu

This instability provides the valve with three properties: (i) The state of the valve is binary ("open" or "closed"), which enables unambiguous control, despite the uncertainties associated with nonlinear and viscoelastic deformation of the elastomers. The valve requires power only while switching between the two states. (ii) The membrane can be designed to be bistable. Bistability allows the fabrication of latching valves, which remain in either open or closed states without an applied pressure. (iii) The snap-through instability is hysteretic. As a result, the valve is resistant to noise and can (in a feedback control scheme) generate periodic pressure oscillations, when connected to a source of constant pressure.

The instability of flexible membranes has previously been used in the design of hard valves (*30*, *31*). In soft robotics, snap-through instabilities are a tool to engineer the response of soft actuators to actuation (*4*, *32*–*34*). The valve presented in this work is different from these examples because it is an entirely soft control element that can be integrated into existing designs for soft, pneumatic actuators. The snap-through instability determines the pressures at which the valve switches. We measured these pressures as a function of the geometry and the material of the valve. We fabricated and characterized a pneumatic switch, a device that switched air flow from two pressure sources, and a pneumatic oscillator, a device that generates periodic motion using a source of constant pressure. Both devices use the soft valve as the functional element.

We demonstrated the ease of implementation and utility of the valve in two applications: (i) A soft gripper, which autonomously grasps objects upon contact. When the "palm" of the gripper contacts the object, the valve is triggered and causes the gripper to close around the ball. An externally applied pressure signal resets the valve, which reopens the gripper. (ii) A soft earthworm, which advances using a source of constant pressure. We integrated the valve into a linear actuator. Connected to a source of constant pressure, the valve periodically inflates and deflates the actuator, which advances because of friction acting asymmetrically on its feet.

The valve can act as a switch for automated functions in soft devices, enabling autonomous feedback and feedforward control in soft actuators. The pressures at which the valve switches can be controlled by changing geometry and material. The design of the valve is simple, modular, and scalable. The ability to generate oscillations inside a robot makes it possible to construct a fully soft, untethered soft robot that can react to stimuli from its environment.

## RESULTS

### The soft, bistable valve

The basic design of the valve uses two instabilities: snap-through instability of a membrane and kinking of a tube (Fig. 1). The two instabilities act cooperatively to control airflow through the valve. In this design, a bistable, hemispherical membrane separates two chambers (Fig. 1, A and B). Elastomeric tubing leads through each chamber. When the membrane is curved downward (state 1), the tubing in the bottom chamber kinks and blocks air flow through it, whereas air flows freely through the tubing in the top chamber. When the membrane is curved upward (state 2), the opposite is true; the tubing in the top chamber kinks and blocks airflow through it, whereas the bottom chamber is open and allows air to flow through freely. The membrane can be switched between the two states by the pressure difference between the bottom ($P_+$, kPa) and top ($P_-$, kPa) chambers ($\Delta P = P_+ - P_-$, kPa).

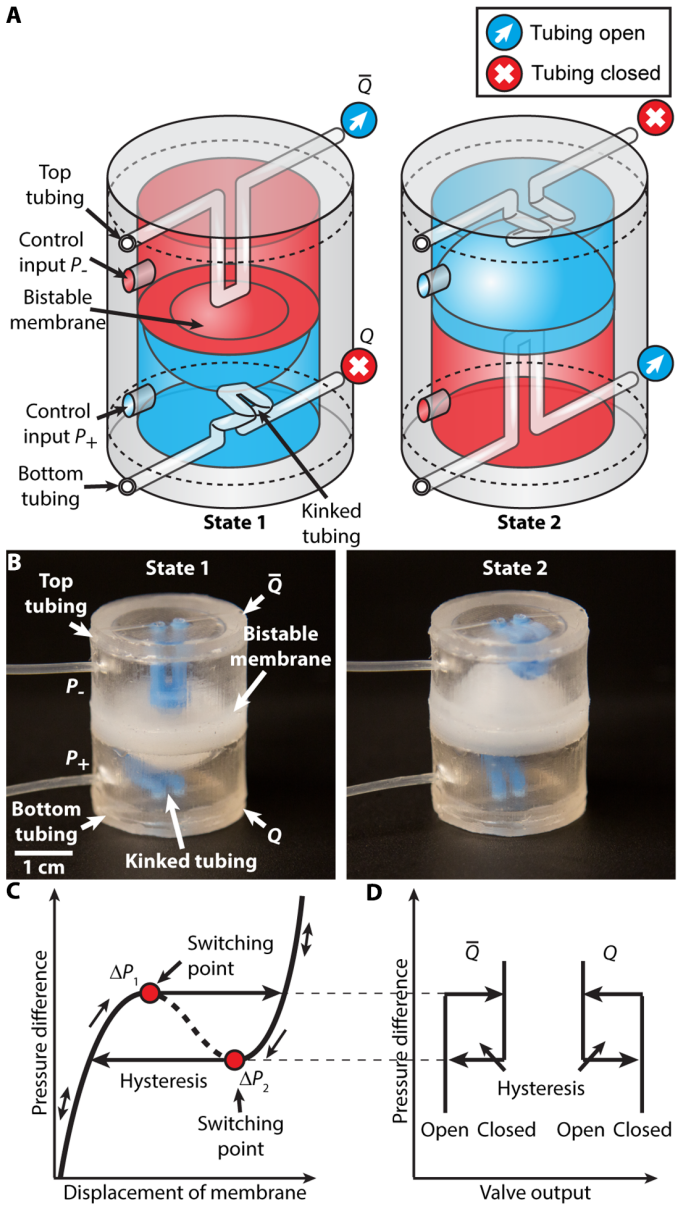


**Fig. 1. Details of the soft, bistable valve.** (**A**) Schematic showing the components of the valve. The valve consists of a hemispherical, elastomeric membrane separating two chambers. Control pressures in the bottom ($P_+$) and top ($P_-$) chambers deform the membrane. When the membrane is in the downward position (state 1), it blocks air flow through a tube leading through the bottom chamber by kinking the tube. When the membrane is in the upward position (state 2), it blocks air flow through the top tube. (**B**) Photographs of the valve in both states. (**C**) When the pressure difference, $\Delta P$, between the two chambers reaches a critical value, $\Delta P_1$, the membrane snaps to the upward position. When the pressure difference decreases below $\Delta P_2$, the membrane snaps back to the downward position. (**D**) The tubing kinks (and un-kinks) during the snapping process. The states of the bottom tubing ($Q$) and the top tubing ($\bar{Q}$) are binary (i.e., open or closed) and hysteretic (movie S1).

We describe this switching behavior using a bifurcation diagram, one axis being the pressure difference $\Delta P$ and the other axis being the displacement of the membrane (Fig. 1C). Initially, when $\Delta P = 0$, the membrane is downward (state 1). As $\Delta P$ increases (i.e., as the bottom chamber is pressurized), the membrane bends toward the top chamber,

and because it is constrained by the walls of the valve, it compresses in area. At the snap-upward pressure $\Delta P_1$ (kPa), the membrane passes through the center of the valve and expands again in the top chamber (state 2). This behavior can—depending on the geometry of the valve—lead to a negative tangential stiffness. When an incompressible fluid (e.g., water) pressurizes the bottom chamber, the pressure decreases upon further deformation (i.e., the dashed line in Fig. 1C). When a compressible gas (e.g., air) is used, the energy stored during compression of the membrane releases, in a dynamic "snapping" motion of the membrane, to the top chamber. When $\Delta P$ decreases, the membrane again has to overcome the constraint of the walls of the valve to return to state 1. To overcome this constraint and snap back to the bottom chamber, the pressure must drop below the snap-downward pressure $\Delta P_2$ (kPa). This type of snap-through instability is well understood and has long been the basis for toy "poppers" (*35*, *36*).

While the membrane is being deformed, the tubing compresses axially. Initially, the tube bends without constricting the air flow (fig. S1). At a critical compression, the walls of the tubing collapse, leading to a kink that blocks air flow (fig. S1). The length of the tubing can be chosen such that the collapse starts and finishes within the snapping motion of the membrane. Coupling these two instabilities leads to binary, opposite states of air flow ("open/closed") through the bottom tubing ($Q$) and the top tubing ($\bar{Q}$), with hysteretic switching behavior (Fig. 1D and movie S1).

When the bistable membrane is integrated into a soft robot, the interior of an actuator can act as one of the "chambers" of the valve. Depending on the application, one of the chambers and/or one of the tubes can be omitted. Because we fabricated the parts of the valve by molding, they can be directly incorporated into the mold for a soft actuator. This integration eliminates the need for additional fabrication techniques.

### Dependence of $\Delta P_1$ and $\Delta P_2$ on the geometry

The critical pressures $\Delta P_1$ and $\Delta P_2$—the pressures at which the membrane switches from one state to the other—depend on the geometry of the membrane and the walls. We studied their dependence on the thickness $H$ (mm) of the membrane and on the inclination angle θ (°)—the angle made between the top surface of the membrane and a plane perpendicular to the wall of the valve (Fig. 2A). We used a syringe pump to pressurize and depressurize the bottom chamber with air while the top chamber was kept at atmospheric pressure and recorded the pressure in the bottom chamber as a function of time (Fig. 2A). From the measured minima and maxima of the pressure-time curves, we determined $\Delta P_1$ and $\Delta P_2$. For some geometries, the membrane did not snap back, even when the pressure in the bottom chamber was reduced to atmospheric pressure (i.e., $\Delta P_2 < 0$). In these cases, we disconnected the syringe pump after the membrane snapped upward and pressurized the top chamber, keeping the bottom chamber at atmospheric pressure.

We studied the dependence of $\Delta P_1$ and $\Delta P_2$ on the thickness of the membrane by varying $H$ from 0.50 to 4.25 mm, using membranes fabricated from Dragon Skin 10 NV elastomer (Smooth-On) with diameter $D$ = 20 mm and θ = 90° (fig. S2). The critical pressure required to snap the membrane upward ($\Delta P_1$) increased with $H$ (Fig. 2B). For $H <$ 3.00 mm, the membrane did not snap back on its own but had to be pushed back to the original position by pressurizing the other chamber (i.e., $\Delta P_2 < 0$). Membranes with 3.0 mm ≤ $H$ ≤ 4.00 mm snapped back when the pressure decreased below a positive critical value, which increased with $H$ until $\Delta P_2$ converged with $\Delta P_1$. For $H >$ 4.00 mm, we did not observe the snap-through instability (i.e., the measured pressure-time curve was monotonic). We note that membranes with

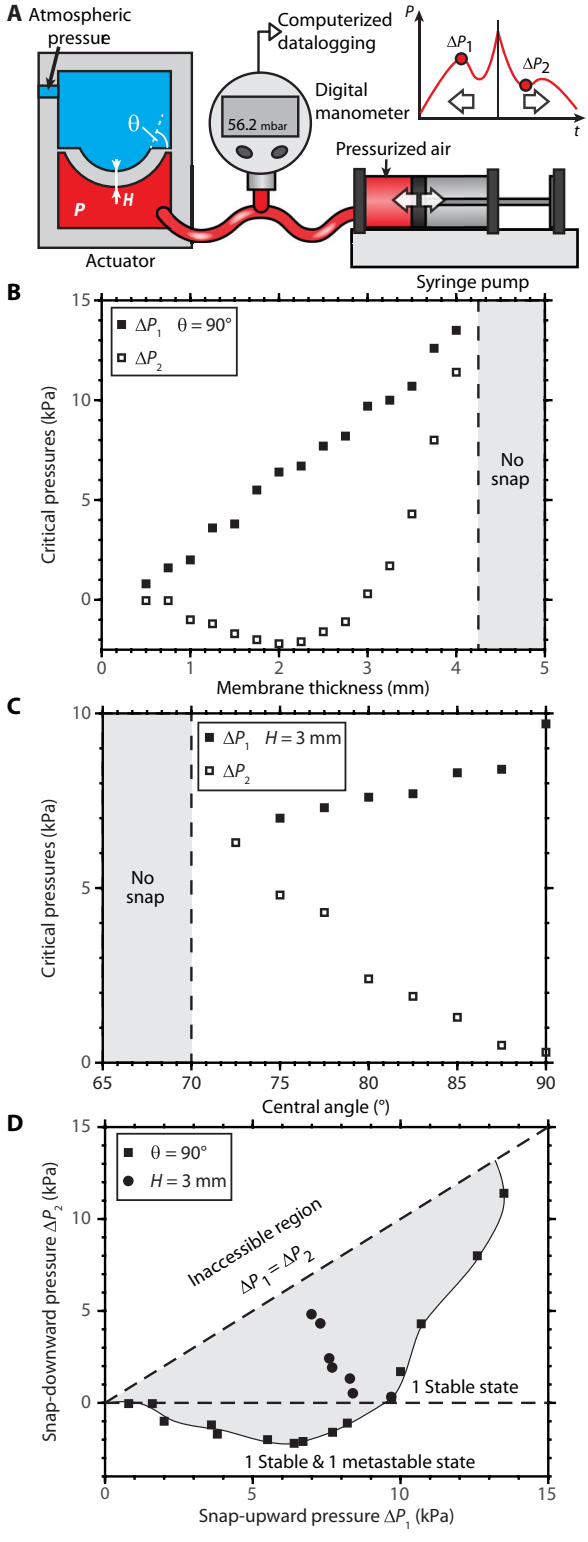


**Fig. 2. Measurements of the critical pressures.** (**A**) Schematic of the apparatus used to measure $\Delta P_1$ and $\Delta P_2$ for different geometries. (**B**) Critical pressures, $\Delta P_1$ and $\Delta P_2$, as a function of $H$. (**C**) Critical pressures, $\Delta P_1$ and $\Delta P_2$, as a function of θ. (**D**) $\Delta P_2$ plotted against $\Delta P_1$ for valves with different $H$ and θ values. The boundary of accessible critical pressures is defined by $\Delta P_2 = \Delta P_1$, and the values of $\Delta P$ for a valve with θ = 90°, and various $H$. Valves with critical switching pressures within this boundary are obtained when θ < 90°.

$H \leq 1.00$ mm did not snap quickly to the other side but transitioned between the states in a slow process during which the pressure did not change.

The behavior of the membrane is a result of two concurrent modes of deformation: (i) compression and (ii) bending of the membrane. The walls impose a barrier that must be overcome by the membrane (by compressing in area) for it to transition to the opposite chamber. This barrier is the origin of the snap-through instability. During the deformation, the membrane also bends. The bending stiffness of the membrane provides a restoring force for the membrane to return to its original position. The bending and compressional stiffness of the membrane both increase with $H$ (the bending stiffness scales faster than the compressional stiffness), and therefore, $\Delta P_1$ increased as $H$ increased. For thin membranes ($H < 3.0$ mm), the restoring force was too small to overcome the constraint of the walls without a pressure from the top chamber (i.e., $\Delta P_2 < 0$). For $H > 3.0$ mm, the restoring force was large enough for the membrane to spontaneously snap back during depressurization ($\Delta P_2 > 0$). When $H$ approached 4.25 mm, the bending stiffness dominated over the compressional stiffness so that the instability disappeared.

We also measured the values of $\Delta P_1$ and $\Delta P_2$ for membranes with θ ranging from 65° to 90° while maintaining $H = 3.0$ mm (Fig. 2C). The angle θ determines how much the membrane must be compressed, in hoop direction, to pass through the center of the valve. Lower values of θ, therefore, led both to smaller $\Delta P_1$ and to smaller differences in the critical switching pressures ($\Delta P_1 - \Delta P_2$). For θ < 70°, we did not observe snap-through. When θ = 70°, the membrane snapped only when depressurizing the bottom chamber. We were also able to reduce $\Delta P_1$ by decreasing the thickness (and thus the stiffness) of the sidewall of the valve, which reduced the constraint on the membrane (fig. S3).

The behavior of the valve changes with the geometry of the membrane (Fig. 2D). The range of achievable switching pressures is defined by the diagonal $\Delta P_2 = \Delta P_1$ (because for the snap-through instability $\Delta P_1 > \Delta P_2$) and the data measured for θ = 90°. Points within this region can be obtained by reducing θ. It is possible to increase the range of switching pressures by using a stiffer elastomer (figs. S4 and S5). However, the size of the valve does not influence the switching pressures (fig. S3). The curve $\Delta P_2 = 0$ splits the $\Delta P_2 - \Delta P_1$ plane into two regions with distinctly different behaviors. In the region where $\Delta P_2 > 0$, the membrane only has one stable state (downward) when $\Delta P = 0$, so it snaps back on its own when $\Delta P$ drops below $\Delta P_2$. These membranes can be used to fabricate nonlatching pneumatic switches. Nonlatching switches would require a continuous pressure signal to remain in the upward state but would not require continuous power because air only flows during the switching process. In the region where $\Delta P_2 < 0$, the membrane also has one metastable state (upward) when $\Delta P = 0$. These membranes can be used to fabricate latching pneumatic switches that require pressure signals only during switching.

## The soft, bistable valve as a switch

Figure 3A shows a soft, bistable valve that acts as a switch between two different sources of constant pressure. The bottom tubing is connected to an air source of pressure $P_S$ (kPa), and the top tubing is connected to the atmosphere, which acts as the second air source. When the membrane is in the downward position, the bottom tubing is kinked so that $P_S$ is disconnected from the output; the top tubing remains open, and the output of the valve is atmospheric pressure (state 1; Fig. 3A). When a control pressure $P_+ > \Delta P_1$ is applied to the bottom chamber, the membrane snaps upward, kinking the top tubing and

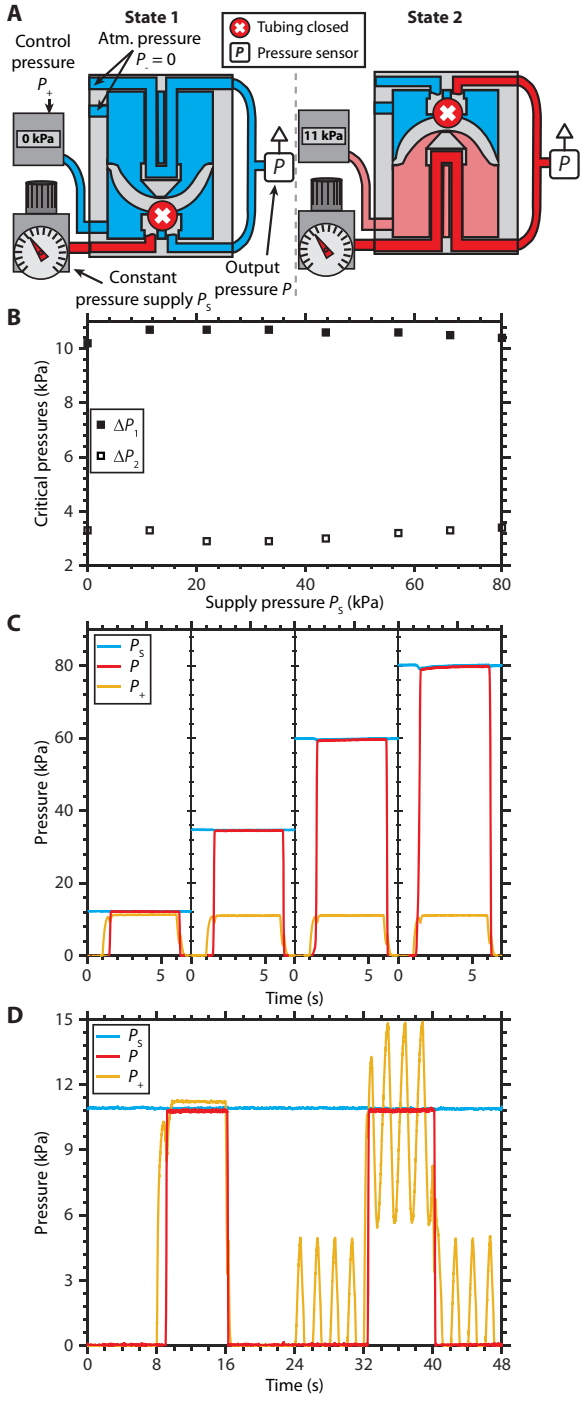


**Fig. 3. Soft, bistable valve acting as a pneumatic switch.** (**A**) The bottom tubing is connected to an air supply of constant pressure $P_S$. The top tubing and the top chamber are connected to the atmosphere. The top and the bottom tubing are joined together behind the valve to form the output $P$ of the pneumatic switch. The pressure in the bottom chamber is controlled by a variable pressure controller ($P_+$). When the membrane bends downward, it kinks the bottom tubing; when it is bent upward, it kinks the top tubing. (**B**) Critical pressures $\Delta P_1$ and $\Delta P_2$ as a function of $P_S$. (**C**) Output of the valve for different $P_S$ values and rectangular pulses as control input ($P_+ = 11$ kPa). (**D**) Response of the valve to two rectangular pulses ($P_+ = 11$ kPa) as the control input. A sinusoidal wave (frequency, 0.5 Hz; amplitude, 5 kPa) is superposed to the second pulse. $H = 3$ mm, θ = 87.5°.

opening the bottom tubing, which connects $P_S$ to the output, while blocking its connection to the atmosphere (state 2; Fig. 3A). When $P_+$ decreases below $\Delta P_2$, the membrane snaps back and switches the output back to the atmosphere.

On the basis of the geometry of the devices of Fig. 2 ($H$ = 3.0 mm, θ = 87.5°), we fabricated a soft valve from Dragon Skin 10 NV, using Smooth-Sil 950 (Smooth-On) for the internal tubing. The presence of the tubing within the valve increased the critical pressures to $\Delta P_1$ = 10.2 kPa and $\Delta P_2$ = 3.3 kPa (Fig. 3B), compared with $\Delta P_1$ = 8.4 kPa and $\Delta P_2$ = 0.5 kPa for membranes without tubing (Fig. 2C). This change in critical pressures arises because the shorter top tubing is more resistant to axial compression than the longer bottom top tubing. The diameter of the membrane on which the control pressure acts is ~10 times larger than the inner diameter of the tubing, on which the supply pressure acts, and thus, we did not observe a measurable change of the critical pressures up to $P_S$ = 80 kPa (Fig. 3B). At pressures above 80 kPa, the pressure dislodged the tubing from the chamber upon switching, which prevented further measurements.

The valve can also be used for signal amplification, because the snap-through instability occurs even when $P_S$ is larger than the critical pressures (Fig. 3B). Figure 3C shows the response of the valve to 5-s-long pressure pulses of $P_+$ = 11 kPa as the input signal and supply pressures $P_S$ up to 80 kPa, which corresponds to a gain (pressure amplification) of 7.3. The delay in switching results mainly from the flow resistance of the tubing between the pressure controller and the valve (the dip in the control pressure corresponds to the onset of the snap-through, during which the pressure decreased because of the volume change of the bottom chamber; the output reached its final state ~0.2 s later).

The hysteresis of the membrane makes the operation of the valve robust to noise and allows the use of the valve as a pneumatic noise filter (a common concept used in digital signal processing). The electronic equivalent to the bistable valve is a Schmitt trigger (*37*). A Schmidt trigger is a hysteretic switch with a continuous input (here, the input is the pressure difference between the bottom and top chambers of the valve) and a binary output (atmospheric pressure or $P_S$). Noise in the control signal only transmits to the output when it is larger than the hysteresis of the Schmidt trigger. To demonstrate this property, we applied two 8-s pressure pulses of $P_+$ = 11 kPa to the bottom chamber of the valve. To simulate noise, we superposed, on the second pulse, a sinusoidal pressure signal (frequency, 0.5 Hz) with an amplitude of about half of the hysteresis (~5 kPa; Fig. 3D). The pressure source could supply only positive pressures, and thus, the negative portion of the sine wave before and after the second pulse was clipped. Because the amplitude of the noise was smaller than the hysteresis of the valve, it did not influence the output pressure (i.e., the valve effectively filtered the noise) (Fig. 3D). When the noise amplitude is larger than the hysteresis, the noise of the control signal transmits to the output (fig. S6).

## A pneumatic gripper for autonomous grasping

We designed a soft gripper that autonomously closes when it contacts an object and can be reopened with an external pressure signal. The gripper consists of five fast pneu-net bending actuators (*38*) arranged circularly around a soft valve, with a contact sensor integrated in the palm of the gripper (Fig. 4A). The contact sensor consists of an elastomeric cap, which surrounds a tube that connects the bottom chamber of the valve to the atmosphere. When an object compresses the cap, the venting tube kinks and blocks the flow of air.

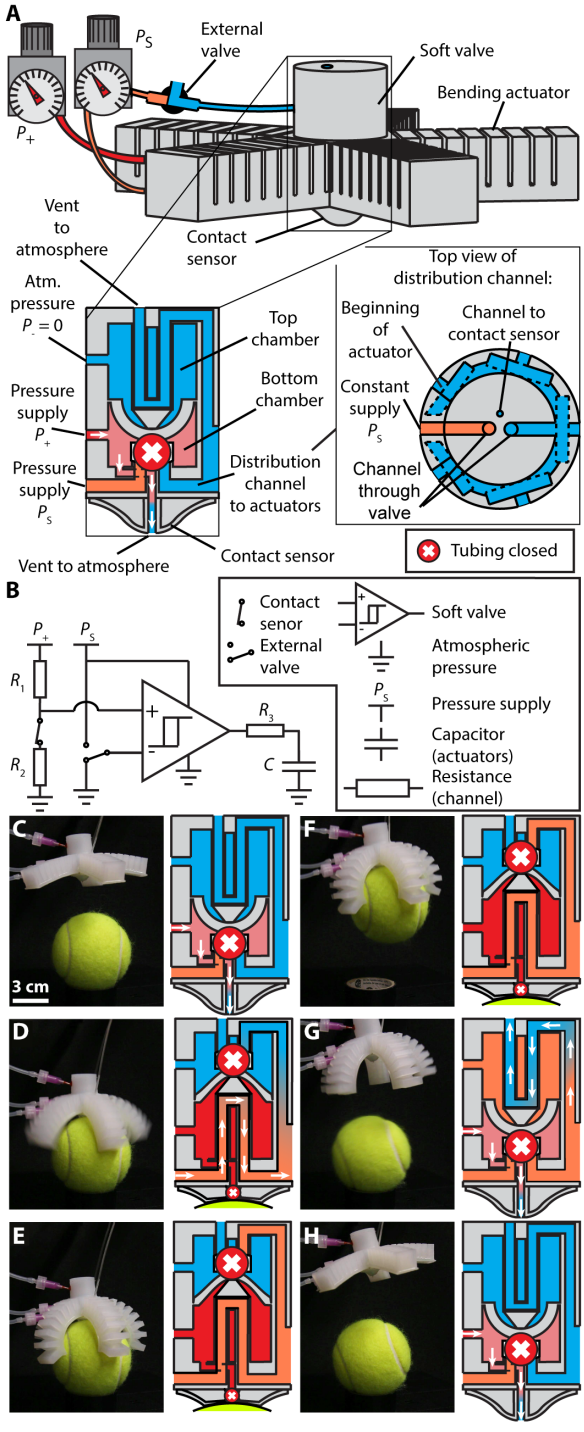


**Fig. 4. Gripper that grasps autonomously.** (**A**) The gripper consists of five bending actuators, connected to a ring-shaped channel, around a soft, bistable valve. When the membrane in the valve is in its downward position, the pressure supply to the ring channel ($P_S$) is blocked, and it is connected to the atmosphere. A second pressure supply ($P_+$) leads to the bottom chamber of the valve and out through the contact sensor at the palm of the hand. The top chamber can be connected through an external valve to the atmosphere or the pressure supply $P_S$. (**B**) Equivalent electrical circuit that represents the pneumatic control in the autonomous gripper. (**C** to **H**) Photographs of the gripper and schematics of the valve autonomously (C to E) closing around a tennis ball and (F to H) releasing the ball (movies S2 and S3).

An air supply (pressure $P_+$, kPa) is connected to the bottom chamber of the valve. A ring channel distributes air to the bending actuators (Fig. 4A). The ring channel is connected, through the bottom tubing of the valve, to a second air supply (pressure $P_S$) and, through the top tubing of the valve, to the atmosphere. When the membrane is in the downward position, the ring channel is connected to the atmosphere, leaving the actuators dormant. When the membrane is in the upward position, the ring channel is connected to $P_S$ and the actuators are pressurized. The pressure supply $P_S$ is also connected to the top chamber, through an external valve, so that pressure in the top chamber can be switched from atmospheric to $P_S$.

We can explain the function of the pneumatic circuit with an analogous electric circuit (Fig. 4B), in which the actuators act as a pneumatic capacitor, the valve acts as a Schmidt trigger, the tubing and the channels act as resistors, and the contact sensor and the external valve act as switches. When the tubing in the contact sensor is open, the electronic switch is closed. Air flows from the pressure source $P_+$ through the bottom chamber of the valve to the atmosphere. The flow resistance of the tubing into and out of the bottom chamber acts as a "voltage" divider so that the pressure in the bottom chamber (positive input of the Schmidt trigger) lies below the switching pressure $\Delta P_1$. When an object kinks the tubing through the contact sensor, the switch in the contact sensor opens, and the pressure inside the bottom chamber increases to $P_+$. The Schmidt trigger switches, and air flows into the capacitor (the fingers of the gripper, which actuate). When we switch the top chamber of the valve (negative input of the Schmidt trigger) to the pressure source $P_S$, the Schmidt trigger switches back, and the capacitor empties to the environment (the fingers of the gripper vent, and the gripper opens).

We fabricated the gripper using Dragon Skin 30 (Smooth-On), Smooth-Sil 950, and Dragon Skin 10 NV. For the air supplies, we used $P_+ = 55$ kPa and $P_S = 69$ kPa. We used the gripper to pick up a tennis ball (movie S2). Before the gripper contacted the ball, air vented through the contact sensor to the environment (Fig. 4C). When the contact sensor touched the ball, the weight of the gripper kinked the tube leading through it (Fig. 4D). The bottom chamber of the valve then pressurized, causing the membrane to snap upward (fig. S7 and movie S3), which connected the bending actuators to $P_S$. From movie S2, we determined that the gripper closed in less than 1 s after contacting the ball. After the gripper was closed (Fig. 4E), we could lift the ball (Fig. 4F). Because the valve is bistable, the gripper stayed closed after picking up the ball, even when the ball moved and was no longer closing the contact sensor. To reset the valve and vent the gripper, we connected the top chamber to the pressure source, $P_S$ (Fig. 4G). The gripper opened in less than 1 s. After switching the top chamber of the valve back to atmosphere (Fig. 4H), we could reuse the gripper (movie S2).

## Feedback control for oscillatory motion using an air source of constant pressure

On the basis of the soft, bistable valve, we designed a soft oscillator that uses an air supply of constant pressure to generate periodic pressure oscillations (Fig. 5A). In this design, the top tubing of the valve is connected to an air supply of pressure $P_S$, and the bottom tubing is connected to the atmosphere. Feedback is established by connecting the bottom tubing and the bottom chamber of the valve (i.e., $P_+ = P$). A vertical channel within the wall of the valve connects the top tubing to the bottom chamber of the valve. To characterize the oscillator, we connected it to a glass jar. Figure 5B shows the electrical analog of the pneumatic circuit.

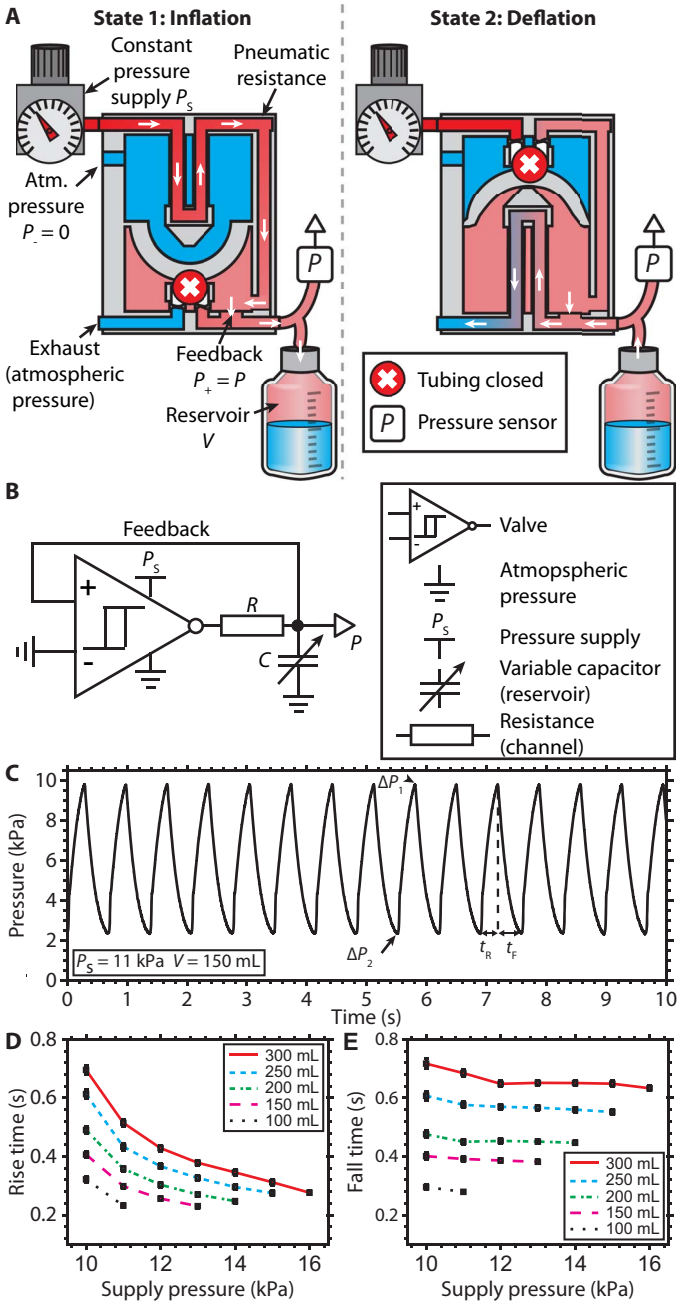


**Fig. 5. Pneumatic oscillator driven by an air source of constant pressure.** (**A**) When the membrane is downward, air flows from the pressure source $P_S$ into a jar of volume $V$, but the tubing between the jar and the atmosphere is blocked. When the pressure $P$ in the bottom chamber exceeds $\Delta P_1$, the membrane snaps upward and blocks air flow from the pressure source $P_S$, and the jar vents to the environment. When $P$ decreases below $\Delta P_2$, the membrane snaps downward, and the jar pressurizes again (movie S4). (**B**) Equivalent electrical circuit that represents the pneumatic feedback control. (**C**) Oscillations in the jar at $P_S = 11$ kPa. (**D**) Rise time ($t_R$) as a function of $P_S$, with different $V$ values. (**E**) Fall time ($t_F$) as a function of $P_S$, with different $V$ values. Error bars in (D) and (E) show the SD of the mean over a 60-s measurement interval. $H = 3$ mm and $\theta = 87.5°$.

When the output pressure of the valve $P$ is smaller than $\Delta P_1$, the membrane bends downward (state 1; Fig. 5A), and air flows from the pressure supply, through the top tubing, to the glass jar. Because of the feedback (Fig. 5B), the membrane snaps upward (state 2; Fig. 5A)

when the pressure in the glass jar exceeds the critical pressure $\Delta P_1$. The glass jar vents through the bottom tubing to the atmosphere until the pressure drops below $\Delta P_2$, at which point the membrane snaps back to state 1. This behavior leads to periodic oscillation of $P$ between $\Delta P_2$ and $\Delta P_1$ (movie S4). Without the instability (i.e., if the transitions between the two states were continuous), the valve would equilibrate in a state in which the tubing through both chambers is partially open so that the air flow into the jar equals the air flow out of the jar and oscillations would not occur.

We fabricated a soft oscillator using Dragon Skin 10 NV for the valve ($H$ = 3 mm, θ = 87.5°) and Smooth-Sil 950 for the internal tubing. We connected the soft oscillator to a glass jar, with a volume of $V$ = 150 ml (we adjusted the volume of the jar by filling it with water). Using a pressure input of $P_S$ = 11 kPa, we recorded the pressure inside the jar as a function of time (Fig. 5C). The valve periodically, and autonomously, pressurized (rise time $t_R$ = 0.3 s) and depressurized (fall time $t_F$ = 0.4 s) the jar, which oscillated between $P$ = 0.24 kPa and $P$ = 0.98 kPa.

Figure 5 (D and E) shows the dependence of $t_R$ and $t_F$ on the supply pressure $P_S$ for capacitors with volumes ($V$) ranging between 100 and 300 ml. The times $t_R$ and $t_F$ scaled with the volume of the capacitor, because less air is required to change the pressure in a smaller volume. Increasing $P_S$ led to smaller values of $t_R$. However, the fall time $t_F$ depends on the pressure difference between the capacitor and the atmosphere at the time the valve switches (i.e., $\Delta P_1$), and because $\Delta P_1$ does not change with $P_S$, $t_F$ was not substantially affected by $P_S$. We observed the fastest oscillations (2 Hz) for $V$ = 100 ml and $P_S$ = 11 kPa and the slowest oscillations (0.7 Hz) for $V$ = 300 ml and $P_S$ = 10 kPa. The lower limit for $P_S$ is determined by the critical pressure, $\Delta P_1$ (here 0.98 kPa), so we observed no oscillations at $P_S$ = 9 kPa. Experimentally, we observed an upper limit for $P_S$, which depended on the volume of the jar (the last data point of each measured curve), when $t_R$ ranged between 0.23 and 0.28 s. Beyond this upper limit, the valve did not oscillate, because the membrane equilibrated to a state in which both channels of the valve were not completely kinked (movie S5 and fig. S8). For volumes $V$ = 50 ml, we did not observe stable oscillations, possibly because $t_R$ was too short, even for $P_S$ = 10 kPa. To test whether the upper limit of $P_S$ is dictated by the duration of $t_R$, we introduced a 2-cm-long tube, with an inner diameter of 0.79 mm, between the pressure supply and the valve to increase the flow resistance. We obtained stable oscillations, even at $P_S$ = 50 kPa and $V$ = 50 ml (fig. S9), suggesting that $t_R$ is the limiting factor and not $P_S$ or $V$.

The compliance of all parts of the valve allows deformation of the valve without damage. An oscillator (operated with $P_S$ = 10 kPa at $V$ = 250 ml) restarted oscillating autonomously after we had crushed it with a 2-kg weight (movie S6). To determine whether the behavior of the valve changes over time, we recorded the oscillations of a valve, using a constant pressure input of $P_S$ = 11 kPa, connected to a glass jar ($V$ = 150 ml). After $10^5$ cycles, we measured a 5% decrease of $\Delta P_1$ and a 3% decrease of the oscillation frequency (fig. S10). The critical pressure $\Delta P_2$ did not change noticeably.

## An autonomous earthworm-like walker

We demonstrate that the valve can be used as a feedback controller for soft robots. Using the soft oscillator, we designed a soft robot with earthworm-like motion that uses air from a source of constant pressure ($P_S$) (Fig. 6A). The critical pressures of the valve determine the pressures between which the robot oscillates. The worm consists of a linear bellows actuator surrounded by a cylindrical sleeve (which acts as a restoring spring). One end of the bellows actuator contains the soft

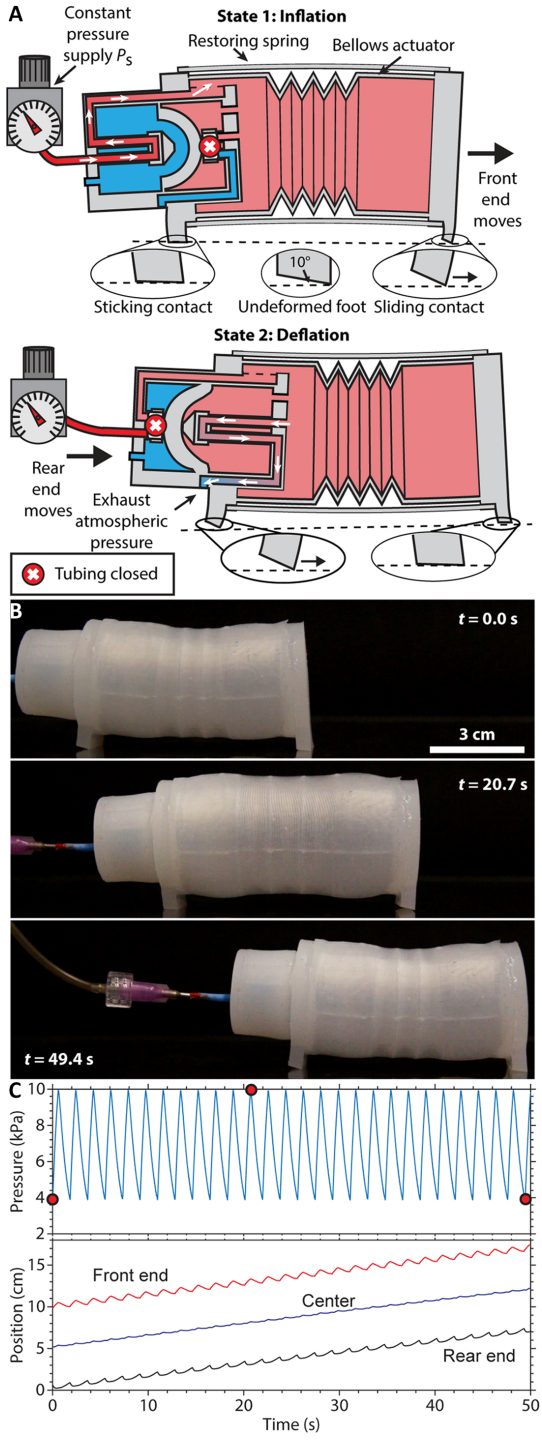


**Fig. 6. Autonomous soft robot with earthworm-like locomotion using an air source of constant pressure.** (**A**) The earthworm consists of a linear bellows actuator with cylindrical sleeve as a restoring spring and a soft, bistable valve, integrated into the rear of the actuator. The design of the valve is the same as that for the pneumatic oscillator, with the bottom chamber of the valve connected to the bellows actuator. The bellows actuator bends upward during inflation and downward during deflation, which causes asymmetric contact between the feet and the ground, leading to asymmetric friction and directional movement. (**B**) Photographs of the moving earthworm at three points in time (movie S7). (**C**) Pressure inside the robot and positions of front end, rear end, and center as a function of time for $P_S$ = 17 kPa. The red dots indicate the times when the photographs in (B) were taken.

oscillator, whereas the other end is capped with an elastomeric disc. Both ends of the robot have elastomeric feet, angled at 10°, to create asymmetric friction during expansion and contraction.

Figure 6B shows snapshots of the earthworm moving on a smooth surface, connected to an air supply of pressure $P_S$ = 17 kPa (movie S7). When the bellows actuator inflated, frictional forces at the feet caused the earthworm to bend upward. This bending caused the front foot to contact the ground with its leading edge only, whereas the back foot touched the ground with its entire surface (Fig. 6A). Thus, the front foot slid forward and the back foot stuck. During deflation, the bellows actuator bent downward so that the front foot stuck and the back foot moved forward (Fig. 6A). Oscillations in the position of the front and back of the actuator are caused, predominantly, by tilting of the ends during bending. The worm stretched and compressed each cycle by 12%, and the worm advanced at a rate of 8.4 cm/min (Fig. 6C). The oscillation period was 1.8 s.

## DISCUSSION

This article describes a design concept for a pneumatic valve that consists entirely of soft components. The valve functions based on a snap-through instability and uses pneumatic signals for control. The valve can be used for latching and nonlatching switches, signal amplifiers, and noise filters. When integrated in a feedback loop, the soft valve can inflate and deflate a soft actuator—autonomously and periodically—using a constant pressure input. The bistable valve achieves these functions in a way that is fundamentally different from the microfluidic logic circuits reported previously (*23*–*26*, *28*): In microfluidic circuits, the complex interplay of pneumatic capacitors, resistors, and valves enables function on a system level; the snap-through instability of a hemispherical membrane and kinking of a tube enable function on the component level. This makes the function of a microfluidic circuit more sensitive to the downstream components (e.g., the soft robot) and its behavior more difficult to predict. In Quake-type valves, which are used in many microfluidic circuits (*23*–*27*), for example, membranes work against the controlled flow. The control pressure therefore depends on the pressure of this flow, and it is not straightforward to achieve a large pressure gain. The control of the bistable valve (the differential pressure across the membrane) is decoupled from the controlled flow (the air flow inside of the tubing). This makes the control pressure independent of the controlled flow, and the mechanical advantage of the membrane on the smaller tubing can provide a large gain (which, in this work, was limited by the strength of the connection between the tubing and the valve).

These comments are not intended to criticize microfluidic systems. Although not demonstrated yet for soft robots, they can theoretically be scaled up to circumvent the difficulties of fabrication and of integration encountered by Wehner *et al.* (*23*) (whereas the bistable valve will be difficult to scale down) and will likely require fewer individual parts than the bistable valve. The bistable valve, on the other hand, allows simpler implementation of some functions. The bistable valve is therefore complementary to the elements of classical microfluidics. On the large scale, both can be combined to achieve a balance of system complexity, robustness of design, and ease of fabrication.

Here, we used a hemispherical membrane as the control element of the valve, but there are other structures that show reversible snap-through behavior and may be equally suitable for autonomous actuation of soft devices (*35*, *39*). We used pneumatic channels that ran parallel to the bistable membrane, although other designs are possible [e.g., feeding the tubing directly through the membrane, to fabricate pressure-release valves, or pressure-limiting valves (fig. S11)]. The two chambers of the valve can be parts of two different actuators, to switch the valve depending on their differential pressure, to obtain coordinated motion.

To fabricate autonomous, untethered, soft robots, the valve may also be used in combination with energy sources that are directly integrated into a soft device (*40*, *41*). If the surrounding walls are designed to maintain structural integrity under negative pressure, the valve may also be used with vacuum. However, if an incompressible fluid (e.g., water) is used to control the valve, the incompressibility of the fluid may prevent the membrane from snapping (in that case, feedforward control is still possible). For the oscillator to work with an incompressible fluid, and a mechanism analogous to that which we describe, the walls of the valve or the soft robot can be designed to provide enough compliance for the snap-through instability to occur.

Although parts of the valves can be directly integrated into the mold of the actuators they control, they still require additional bonding steps during assembly. We envision that, by using a 3D printer that prints elastomeric materials, an entirely soft actuator, including the control elements, could be printed as one monolithic piece (*23*, *42*–*44*). Another limitation of the bistable valve is that $\Delta P_1$ and $\Delta P_2$ do not depend only on the geometry and material of the membrane and the tubing but also on the surrounding structure. To obtain the desired switching behavior, one has to design the membrane together with the soft actuators. The mechanics of the snap-through instability is well understood so that computational models (e.g., a finite element simulation) can aid the design and optimization of the geometry of the membrane. The characterization performed in this work (Fig. 2 and fig. S3) gives general guidelines for how changes in geometry influence the switching pressures.

Elastomers allow large and repeated deformation without failure. The snap-through instability makes the control digital and unambiguous, unaffected by the uncertainties associated with nonlinear and viscoelastic deformation or by small perturbations from the external environment. Through the automatic gripper and the autonomous "earthworm," we demonstrate that simple logic and control elements can be directly integrated into soft robots; this integration decreases their dependence on hard control elements and is a step toward the design and fabrication of entirely soft, complex, autonomous robots.

## MATERIALS AND METHODS

### Objectives and design of the study

The objective of this study is to demonstrate that elastic instabilities can be used to control airflow in soft robots and enable automated functions. Structures that have instabilities can be directly integrated into the design of the actuators and fabricated with the same tools (molding). Here, we used a hemispherical membrane because it is easy to fabricate and has minimal geometric parameters. We used the autonomous gripper and the autonomous earthworm as practical examples for feedforward and feedback control with the soft valve.

### Fabrication of samples

All parts were casted in the 3D printed molds (Stratasys Dimension Elite, Stratasys Objet30). Input files for the 3D printer for all molds are provided in the Supplementary Materials (data files S1 to S6). We used the elastomers Dragon Skin 10 NV, Dragon Skin 30, Ecoflex 30, and Smooth-Sil 950 (all Smooth-On) as materials. The Supplementary Materials contains a description of the preparation of the pre-polymer solutions, the assembly of the molds, the casting process, and a step-by-step description of the fabrication.

### Testing methods

We pressurized the devices for the measurements of the critical pressures with a Harvard PHD ULTRA syringe pump and measured the pressures with a LEX 1 (KELLER) pressure sensor. The pressures for the characterization of the pneumatic switch were regulated with ITV0010-2BL (SMC Pneumatics) electro-pneumatic pressure regulators, and the pressures were measured with ADP5151 (Panasonic Electronic Components) pressure sensors. We controlled the input pressures for the automatic gripper, the soft oscillator, and the walker by regulating an in-house air supply manually. As external valves, we used manually controlled needle valves and ITV0010-2BL regulators. We recorded the pressures with the LEX 1 sensors and a U5244-000002-002BA sensor (TE Connectivity). The data of the LEX 1 sensor were recorded with its software. All other control and recording was done through a DAQ card (NI USB-6218) on a PC by MATLAB. The Supplementary Materials contains detailed descriptions of each experiment.

## SUPPLEMENTARY MATERIALS

robotics.sciencemag.org/cgi/content/full/3/16/eaar7986/DC1
Materials and Methods
Fig. S1. Kinking of tubing.
Fig. S2. Geometry of devices for measuring the critical pressures.
Fig. S3. Critical pressures as functions of wall thickness and scale.
Fig. S4. Critical pressures as a function of the shear modulus.
Fig. S5. Material characterization.
Fig. S6. Influence of large input noise on the output.
Fig. S7. Gripper with a valve without a top chamber.
Fig. S8. Oscillator in intermediate state.
Fig. S9. Oscillations at large input pressures with an additional pneumatic resistance.
Fig. S10. Characterization of soft oscillator after $10^5$ cycles.
Fig. S11. Alternative designs.
Fig. S12. Molds for the devices for measuring the critical pressures.
Fig. S13. Assembly of the devices for measuring the critical pressures.
Fig. S14. Molds for the tubing used inside the chambers of the valves.
Fig. S15. Assembly of the tubing used inside the chambers of the valve.
Fig. S16. Molds for the transparent valve.
Fig. S17. Assembly of the transparent valve.
Fig. S18. Molds for the pneumatic switch.
Fig. S19. Assembly of the pneumatic switch.
Fig. S20. Molds for the autonomous gripper.
Fig. S21. Assembly of the autonomous gripper.
Fig. S22. Molds for the oscillator.
Fig. S23. Assembly of the oscillator.
Fig. S24. Molds for the earthworm-like walker.
Fig. S25. Assembly of the earthworm-like walker.
Movie S1. Switching with the soft, bistable valve.
Movie S2. Autonomous grasping with the soft autonomous gripper.
Movie S3. Soft autonomous gripper without a top chamber.
Movie S4. Soft oscillator.
Movie S5. Soft oscillator equilibrating in intermediate state.
Movie S6. Soft oscillator restarts after crushing.
Movie S7. Autonomous earthworm-like walker.
Data file S1. Molds for the devices to measure the critical pressures.
Data file S2. Molds for the tubing used inside of the chambers of the valve.
Data file S3. Molds for the transparent valve.
Data file S4. Molds for the pneumatic switch.
Data file S5. Molds for the autonomous gripper.
Data file S6. Molds for the oscillator.
Data file S7. Molds for the earthworm-like walker.
Reference (*45*)

## REFERENCES AND NOTES


1. F. Ilievski, A. D. Mazzeo, R. F. Shepherd, X. Chen, G. M. Whitesides, Soft robotics for chemists. *Angew. Chem. Int. Ed.* **50**, 1890–1895 (2011).
2. R. F. Shepherd, F. Ilievski, W. Choi, S. A. Morin, A. A. Stokes, A. D. Mazzeo, X. Chen, M. Wang, G. M. Whitesides, Multigait soft robot. *Proc. Natl. Acad. Sci. U.S.A.* **108**, 20400–20403 (2011).
3. R. V. Martinez, C. R. Fish, X. Chen, G. M. Whitesides, Elastomeric Origami: Programmable paper-elastomer composites as pneumatic actuators. *Adv. Funct. Mater.* **22**, 1376–1384 (2012).
4. D. Yang, M. S. Verma, J.-H. So, B. Mosadegh, C. Keplinger, B. Lee, F. Khashai, E. Lossner, Z. Suo, G. M. Whitesides, Buckling pneumatic linear actuators inspired by muscle. *Adv. Mater. Technol.* **1**, 1600055 (2016).
5. X. Gong, K. Yang, J. Xie, Y. Wang, P. Kulkarni, A. S. Hobbs, A. D. Mazzeo, Rotary actuators based on pneumatically driven elastomeric structures. *Adv. Mater.* **28**, 7533–7538 (2016).
6. C. Laschi, B. Mazzolai, M. Cianchetti, Soft robotics: Technologies and systems pushing the boundaries of robot abilities. *Sci. Robot.* **1**, eaah3690 (2016).
7. P. Polygerinos, Z. Wang, K. C. Galloway, R. J. Wood, C. J. Walsh, Soft Robotic glove for combined assistance and at-home rehabilitation. *Rob. Auton. Syst.* **73**, 135–143 (2015).
8. P. Polygerinos, N. Correll, S. A. Morin, B. Mosadegh, C. D. Onal, K. Petersen, M. Cianchetti, M. T. Tolley, R. F. Shepherd, Soft robotics: Review of fluid-driven intrinsically soft devices; manufacturing, sensing, control, and applications in human-robot interaction. *Adv. Eng. Mater.* **19**, 1700016 (2017).
9. D. Rus, M. T. Tolley, Design, fabrication and control of soft robots. *Nature* **521**, 467–475 (2015).
10. A. De Greef, P. Lambert, A. Delchambre, Towards flexible medical instruments: Review of flexible fluidic actuators. *Precis. Eng.* **33**, 311–321 (2009).
11. H. Zhao, K. O'Brien, S. Li, R. F. Shepherd, Optoelectronically innervated soft prosthetic hand via stretchable optical waveguides. *Sci. Robot.* **1**, eaai7529 (2016).
12. F. Connolly, C. J. Walsh, K. Bertoldi, Automatic design of fiber-reinforced soft actuators for trajectory matching. *Proc. Natl. Acad. Sci. U.S.A.* **114**, 51–56 (2017).
13. Y.-L. Park, B.-R. Chen, R. J. Wood, Design and fabrication of soft artificial skin using embedded microchannels and liquid conductors. *IEEE Sens. J.* **12**, 2711–2718 (2012).
14. R. A. Bilodeau, E. L. White, R. K. Kramer, Monolithic fabrication of sensors and actuators in a soft robotic gripper, in *2015 IEEE/RSJ International Conference on Intelligent Robots and Systems (IROS)*, Hamburg, Germany, 28 September to 2 October 2015 (IEEE, 2015).
15. J.-Y. Sun, C. Keplinger, G. M. Whitesides, Z. Suo, Ionic skin. *Adv. Mater.* **26**, 7608–7614 (2014).
16. C. Paul, Morphological computation: A basis for the analysis of morphology and control requirements. *Rob. Auton. Syst.* **54**, 619–630 (2006).
17. P. Paoletti, G. W. Jones, L. Mahadevan, Grasping with a soft glove: Intrinsic impedance control in pneumatic actuators. *J. R. Soc. Interface* **14**, 20160867 (2017).
18. M. T. Tolley, R. F. Shepherd, B. Mosadegh, K. C. Galloway, M. Wehner, M. Karpelson, R. J. Wood, G. M. Whitesides, A resilient, untethered soft robot. *Soft Robot.* **1**, 213–223 (2014).
19. N. Napp, B. Araki, M. T. Tolley, R. Nagpal, R. J. Wood, Simple passive valves for addressable pneumatic actuation, in *2014 IEEE International Conference on Robotics and Automation (ICRA)*, Hong Kong, China, 31 May to 7 June 2014 (IEEE, 2014).
20. A. D. Marchese, C. D. Onal, D. Rus, Soft robot actuators using energy-efficient valves controlled by electropermanent magnets, in *2011 IEEE/RSJ International Conference on Intelligent Robots and Systems (IROS)*, San Francisco, CA, 25 to 30 September 2011 (IEEE, 2011).
21. B. Mosadegh, A. D. Mazzeo, R. F. Shepherd, S. A. Morin, U. Gupta, I. Z. Sani, D. Lai, S. Takayama, G. M. Whitesides, Control of soft machines using actuators operated by a Braille display. *Lab Chip* **14**, 189–199 (2014).
22. R. F. Shepherd, A. A. Stokes, J. Freake, J. Barber, P. W. Snyder, A. D. Mazzeo, L. Cademartiri, S. A. Morin, G. M. Whitesides, Using explosions to power a soft robot. *Angew. Chem. Int. Ed.* **52**, 2892–2896 (2013).
23. M. Wehner, R. L. Truby, D. J. Fitzgerald, B. Mosadegh, G. M. Whitesides, J. A. Lewis, R. J. Wood, An integrated design and fabrication strategy for entirely soft, autonomous robots. *Nature* **536**, 451–455 (2016).
24. B. Mosadegh, C.-H. Kuo, Y.-C. Tung, Y.-s. Torisawa, T. Bersano-Begey, H. Tavana, S. Takayama, Integrated elastomeric components for autonomous regulation of sequential and oscillatory flow switching in microfluidic devices. *Nat. Phys.* **6**, 433–437 (2010).
25. M. Rhee, M. A. Burns, Microfluidic pneumatic logic circuits and digital pneumatic microprocessors for integrated microfluidic systems. *Lab Chip* **9**, 3131–3143 (2009).
26. Q. Zhang, M. Zhang, L. Djeghlaf, J. Bataille, J. Gamby, A.-M. Haghiri-Gosnet, A. Pallandre, Logic digital fluidic in miniaturized functional devices: Perspective to the next generation of microfluidic lab-on-chips. *Electrophoresis* **38**, 953–976 (2017).
27. M. A. Unger, H.-P. Chou, T. Thorsen, A. Scherer, S. R. Quake, Monolithic microfabricated valves and pumps by multilayer soft lithography. *Science* **288**, 113–116 (2000).
28. P. N. Duncan, S. Ahrar, E. E. Hui, Scaling of pneumatic digital logic circuits. *Lab Chip* **15**, 1360–1365 (2015).
29. D. C. Duffy, J. C. McDonald, O. J. A. Schueller, G. M. Whitesides, Rapid prototyping of microfluidic systems in poly(dimethylsiloxane). *Anal. Chem.* **70**, 4974–4984 (1998).
30. C. Goll, W. Bacher, B. Bürstgens, D. Maas, W. Menz, W. K. Schomburg, Microvalves with bistable buckled polymer diaphragms. *J. Micromech. Microeng.* **6**, 77–79 (1996).

31. M. Gomez, D. E. Moulton, D. Vella, Passive control of viscous flow via elastic snap-through. *Phys. Rev. Lett.* **119**, 144502 (2017).
32. J. T. B. Overvelde, T. Kloek, J. J. A. D'haen, K. Bertoldi, Amplifying the response of soft actuators by harnessing snap-through instabilities. *Proc. Natl. Acad. Sci. U.S.A.* **112**, 10863–10868 (2015).
33. C. Keplinger, T. Li, R. Baumgartner, Z. Suo, S. Bauer, Harnessing snap-through instability in soft dielectrics to achieve giant voltage-triggered deformation. *Soft Matter* **8**, 285–288 (2012).
34. J. Shim, C. Perdigou, E. R. Chen, K. Bertoldi, P. M. Reis, Buckling-induced encapsulation of structured elastic shells under pressure. *Proc. Natl. Acad. Sci. U.S.A.* **109**, 5978–5983 (2012).
35. A. Pandey, D. E. Moulton, D. Vella, D. P. Holmes, Dynamics of snapping beams and jumping poppers. *Europhys. Lett.* **105**, 24001 (2014).
36. P. B. Gonçalves, D. Pamplona, P. B. C. Teixeira, R. L. C. Jerusalmi, I. A. Cestari, A. A. Leirner, Dynamic non-linear behavior and stability of a ventricular assist device. *Int. J. Solids Struct.* **40**, 5017–5035 (2003).
37. P. Horowitz, W. Hill, *The Art of Electronics* (Cambridge Univ. Press, 1989).
38. B. Mosadegh, P. Polygerinos, C. Keplinger, S. Wennstedt, R. F. Shepherd, U. Gupta, J. Shim, K. Bertoldi, C. J. Walsh, G. M. Whitesides, Pneumatic Networks for soft robotics that actuate rapidly. *Adv. Funct. Mater.* **24**, 2163–2170 (2014).
39. A. N. Gent, Elastic instabilities in rubber. *Int. J. Non-Linear Mech.* **40**, 165–175 (2005).
40. C. D. Onal, X. Chen, G. M. Whitesides, D. Rus, Soft mobile robots with on-board chemical pressure generation, in *Springer Tracts in Advanced Robotics* (Springer, 2017), vol. 100, pp. 525–540.
41. M. Wehner, M. T. Tolley, Y. Mengüç, Y.-L. Park, A. Mozeika, Y. Ding, C. Onal, R. F. Shepherd, G. M. Whitesides, R. J. Wood, Pneumatic energy sources for autonomous and wearable soft robotics. *Soft Robot.* **1**, 263–274 (2014).
42. R. L. Truby, J. A. Lewis, Printing soft matter in three dimensions. *Nature* **540**, 371–378 (2016).
43. B. N. Peele, T. J. Wallin, H. Zhao, R. F. Shepherd, 3D printing antagonistic systems of artificial muscle using projection stereolithography. *Bioinspir. Biomim.* **10**, 055003 (2015).
44. R. D. Sochol, E. Sweet, C. C. Glick, S. Venkatesh, A. Avetisyan, K. F. Ekman, A. Raulinaitis, A. Tsai, A. Wienkers, K. Korner, K. Hanson, A. Long, B. J. Hightower, G. Slatton, D. C. Burnett, T. L. Massey, K. Iwai, L. P. Lee, K. S. J. Pister, L. Lin, 3D printed microfluidic circuitry *via* multijet-based additive manufacturing. *Lab Chip* **16**, 668–678 (2016).
45. L. R. G. Treloar, *The Physics of Rubber Elasticity* (Clarendon, ed. 3, 1975).


**Acknowledgments:** We thank J. C. Weaver for help with printing the molds for the transparent valve. **Funding:** The research presented in this paper was funded by the Department of Energy, Office of Basic Energy Sciences, Division of Materials Science and Engineering under award ER45852. P.R. and Z.S. acknowledge support from the Harvard Materials Research Science and Engineering Center supported by the NSF (DMR 14-20570). A.A. thanks the Swedish Research Council (VR) for a postdoctoral fellowship. L.B. is funded by a Natural Sciences and Engineering Research Council of Canada Postdoctoral Fellowship from the Government of Canada. **Author contributions:** P.R., A.A., and G.M.W. developed the concept. P.R., A.A., D.J.P., Z.S., and G.M.W. designed the experiments. P.R., L.B., and S.K. fabricated and characterized the devices to measure the critical pressures. L.B. and D.J.P. fabricated and characterized the pneumatic switch. P.R., A.A., and L.B. fabricated and characterized the soft gripper. P.R., A.A., L.B., and D.J.P. fabricated and characterized the soft oscillator. P.R. and A.A. fabricated and characterized the earthworm. Z.S. and G.M.W. supervised the experiments. P.R., L.B., and G.M.W. wrote the manuscript. A.A., S.K., and Z.S. edited the manuscript. **Competing interests:** G.M.W. owns equity in Soft Robotics Inc. and is a member of its board of directors. Soft Robotics Inc. develops soft robots. P.R., A.A., L.B., Z.S., and G.M.W. filed a patent application (no. 62/607,509) for the soft valve. The other authors declare that they have no competing interests. **Data and materials availability:** All data needed to evaluate the study are presented in the main text or the Supplementary Materials. Contact G.M.W. for any questions regarding experimental raw data.

Submitted 23 December 2017
Accepted 26 February 2018
Published 21 March 2018
10.1126/scirobotics.aar7986

**Citation:** P. Rothemund, A. Ainla, L. Belding, D. J. Preston, S. Kurihara, Z. Suo, G. M. Whitesides, A soft, bistable valve for autonomous control of soft actuators. *Sci. Robot.* **3**, eaar7986 (2018).

Science Robotics

# A soft, bistable valve for autonomous control of soft actuators

Philipp Rothemund, Alar Ainla, Lee Belding, Daniel J. Preston, Sarah Kurihara, Zhigang Suo, and George M. Whitesides

*Sci. Robot.* **3** (16), eaar7986. DOI: 10.1126/scirobotics.aar7986







*Science Robotics* (ISSN 2470-9476) is published by the American Association for the Advancement of Science. 1200 New York Avenue NW, Washington, DC 20005. The title *Science Robotics* is a registered trademark of AAAS.